Supplementary Information for

Mode-of-action profiling reveals glutamine synthetase as a collateral metabolic vulnerability of *M.tuberculosis* to bedaquiline

Zhe Wang[1], Vijay Soni[1], Gwendolyn Marriner[2], Takushi Kaneko[3], Helena I. M. Boshoff[2], Clifton E. Barry III[2] and Kyu Y. Rhee[1*]

[1] Division of Infectious Diseases, Weill Department of Medicine, Weill Cornell Medical College, NY, NY 10065, USA.

[2] Tuberculosis Research Section, Laboratory of Clinical Infectious Diseases, National Institute of Allergy and Infectious Diseases, National Institutes of Health, Bethesda, Maryland 20892, USA.

[3] Global Alliance for TB Drug Development, NY, NY 10005, USA.

*Correspondence to: kyr9001@med.cornell.edu

This PDF file includes:

SI Materials and Methods
Figs. S1 to S23
Captions for Tables S1 to S6

Other supplementary materials for this manuscript include the following:

Table S1 to S6

SI Materials and Methods

Synthesis of BDQ and BDQi. The modification of preparation of bedaquiline and its enantiomer is that the nucleophilic addition to the ketone to form the tertiary alcohol described in the following paragraphs: THF was purchased as anhydrous grade from Sigma-Aldrich. *n*-Butyllithium was purchased as a 2.5 M solution in hexanes from Sigma-Aldrich and titrated prior to use. All other reagents were purchased from Sigma-Aldrich and used without further purification. In a 500 mL oven dried, Ar flushed, round-bottomed flask, diisopropylamine (122 mmol, 17.4 mL, 1 eq) was diluted in anhydrous THF (to 2.3 M, 53 mL) to give a colorless solution. This solution was cooled to -20 °C using a bath of salt water/ice. *n*-Butyllithium (53 mL, 122 mmol, 1 eq) was added dropwise. This solution was stirred 1 h at -20 °C, followed by dilution with THF (54 mL) and cooling to -78 °C using an isopropanol/dry ice bath. A solution of 3-benzyl-6-bromo-2-methoxyquinoline (40 g, 122 mmol, 1 eq) in THF (58 mL) was added dropwise. The reaction was transferred to a -78 °C freezer for approximately 16-20 h. This anionic solution, deep purple in color, was transferred slowly via cannula onto a solution of 3-(benzyl(methyl)amino)-1-(naphthalen-1-yl) propan-1-one (37.0 g, 122 mmol, 1 eq) in THF (0.51 M, 241 mL) in a 1 L oven-dried, Ar-flushed, roundbottomed flask at -70 °C (isopropanol/dry ice bath). The purple reaction was allowed to stir for 2 h with aliquots for LC/MS taken every hour for analysis. This reaction was quenched by slow addition to a solution of acetic acid (24 mL, 305 mmol, 2.5 eq) in THF (10 M, 40 mL), cooled to <10 °C in an ice/water bath, maintaining the temperature during the entire addition. The reaction turned bright orange upon quench. The mixture was purified by flash column chromatography on silica in 50% ethyl acetate/hexane (or a gradient of 25-50% ethyl acetate/hexane) to obtain the desired diastereomer in yields comparable to those reported.

The synthesized BDQ and BDQi are next characterized by HPLC and NMR methods. In detail, the chromatography was performed on an Agilent 1100 HPLC system (comprised of G1322A degasser, G1312A Binary Pump, G1329A autosampler, G1316A column compartment) coupled to a diode array detector (DAD) Agilent G1315A. Mass spectrometry of the UV-vis peak was confirmed with an Agilent G1946D SL mass selective detector utilizing ESI in positive mode. NMR data was acquired on a Bruker 500 MHz spectrometer. Chemical shifts are reported in parts per million (δ). ^{1}H and ^{13}C NMR spectra are referenced to solvent.

MIC and CFU assays. MICs of antibiotics in Mtb were measured using 24-well plates (in agar plate) and 96-well plates (in liquid medium), respectively. In agar plates, 10 µl of Mtb at an OD_{580} of 1.0 were added to each well and placed at 37 °C for 3 weeks. In liquid medium, a low inoculum of Mtb (OD_{580} of 0.02) was added to each well and placed at 37 °C for measurements of turbidity every 3 or 4 days. The minimal antibiotic concentration which totally inhibited Mtb growth was determined as the experimental MIC. CFU growth assays were performed in 96-well plates. Mtb was diluted to an OD_{580} of 0.02 (1 x 10^7 cells/ml) in 7H9 in each well. Antibiotics and other supplements were added as described concentrations and incubated for the indicated periods. Bacterial cultures were then serially diluted in 7H9 broth and plated on 7H10 agar plates, incubated for three weeks at 37 °C and colonies counted by hand.

Drug synergy evaluation. In brief, a matrix of 2 drug concentration ranges was sat up across the rows and columns of a 96-well plate. IC_{50} values were calculated by determining the OD_{580} value 10 days after initial drug inoculation. The raw fitness of growth values, T, from each treated well were converted to inhibition values, Z = (1-T/V), relative to the median V of DMSO-treated wells in the same plate. Drug synergy was identified by comparing the observed effect of drug combinations to those of the single agents. The synergy score is the “highest single agent” Z_{HSA} = max (Z_X, Z_Y), the maximum single-agent response at the corresponding concentrations.

Metabolite extraction. Mtb metabolomes were quenched by plunging Mtb -laden filters into a mixture of acetonitrile/methanol/H_2O (40:40:20) precooled to -40 °C on dry ice. Metabolites were next extracted by mechanical

lysis with 0.1 mm Zirconia beads in a Precellys tissue homogenizer for 3 min (6,500 rpm) twice under continuous cooling at or below 2 °C. Lysates were clarified by centrifugation and then filtered across a 0.22 µm filter. Biomass of each sample was quantified by measuring residual protein/peptide content using a colorimetric assay (Pierce BCA Protein Assay).

Liquid chromatography-mass spectrometry. Extracted metabolites were separated on a Cogent Diamond Hydride type C column. Two different separation programs were used to cover different classes of metabolites. Mobile phase 1 (which was used for detection of non-nucleotide polar metabolites) included the following: solvent A (ddH_2O with 0.2% formic acid) and solvent B (acetonitrile with 0.2% formic acid). The gradient was: 0-2 min, 85% B; 3-5 min, 80% B; 6-7 min, 75% B; 8-9 min, 70% B; 10-11.1 min, 50% B; 11.1-14 min 20% B; 14.1-24 min 5% B with a 10 min re-equilibration period at 85% B at a flow rate of 0.4 ml/min. Mobile phase 2 (used to detect phosphorylated metabolites and nucleotides) consisted of the following: solvent A (ddH_2O with 0.05% ammonium acetate) and solvent B (90% acetonitrile, 10% ddH_2O with 0.05% ammonium acetate). The gradient is: 0-1 min, 95% B; 8-9 min, 80% B; 10-10.5, 50% B; 14-19, 95% with a 15 min re-equilibration period at 100% B at a flow rate of 0.4 ml/min.

The liquid chromatography system was coupled to an Agilent Accurate Mass 6220 TOF or 6520 qTOF mass spectrometer, and the isocratic pump was used for continuous injection of a reference mass solution to achieve the dynamic mass axis calibration. Detected ions were classified as annotated metabolites based on unique, accurate mass-retention time identifiers for masses showing the assumed distribution of accompanying isotopomers. Metabolites were identified using Agilent Quantitative Analysis software and Agilent Profinder software with a mass tolerance of < 0.005 Da. Calibration curves were generated from chemical standards spiked into control Mtb extract to correct for the ion suppression effects.

Recombinant Mtb GS expression, purification, and enzymatic assays. *E. coli* was grown at 37 °C in LB medium to mid-log phase, after which 0.2% L-arabinose was added to induce expression for 3h. After that, cells were collected by centrifugation (8,000 rpm x 10 min), and the cell pellet washed with lysis buffer (20 mM TEA, pH 7.8/300 mM NaCl/30mM imidazole).

For protein purification, the above cell pellet was resuspended in lysis buffer with 5 µg/ml DNase I and then lysed by a high-pressure homogenizer (EmulsiFlex-C5, Avestin Inc, Canada). The supernatant including the soluble fraction was recovered by high-speed centrifugation (12,000 rpm x 15 min), and incubated with pre-equilibrated Ni-NTA agarose (Qiagen, Valencia, CA) for 1 h at 4 °C. Mtb GS was purified through AKTA pure chromatography system (GE Healthcare, USA), using the following elution buffer: 20 mM TEA, pH 7.8/300 mM NaCl/500 mM imidazole. The eluted protein was next dialyzed (Slide-A-Lyzer dialysis cassettes, 10Kd, ThermoFisher Scientific, USA) overnight at 4 °C.

Mtb GS activity was detected by monitoring the ion intensity of glutamine by LC-MS, under the different reaction conditions. The basic reaction mixture (100 µl for each) includes: 50 mM Tris-HCl pH 8.0/ 3 mM Glutamate/ 3 mM NH_4Cl/ 3 mM $MgCl_2$/ 3 mM ATP/ 0.8 µM Mtb GS. Reactions were incubated for 30 min at 30 °C, and then quenched by adding 100 µl precooled MS solvent B (acetonitrile with 0.2% formic acid).

Bioinformatics analysis and data visualization. Ion intensities of individual metabolites were extracted from the raw data file using Quantitative Analysis 6.0 (Agilent Technologies, USA) and Profinder 8.0 (Agilent Technologies, USA) and normalized by each sample's protein concentration. Normalized data then underwent a log_2 transformation, and were imported into Cluster 3.0 (Stanford University, USA) for hierarchical analysis and visualization in heatmap format using Java TreeView 3.0 (Stanford University, USA). Metabolic pathway enrichment analysis was carried out using the online

analytical tool MetaboAnalyst 3.0 (www.metaboanalyst.ca). Gene pathway enrichment analysis was carried out using online analytic tool Gene Ontology Consortium (http://www.geneontology.org/). Metabolic pathway mapping was conducted using the online analytical tool KEGG Mapper (http://www.genome.jp/kegg/pathway.html). The waterfall plot of metabolic correlation network was built and visualized using Excel, based on the calculated pairwise Pearson correlation coefficients from BDQ treated time-dependent and dose-dependent metabolic profiles. Antibiotics IC_{50} values, Km and Vmax values were calculated using Prism 7.0 (GraphPad Software, USA).

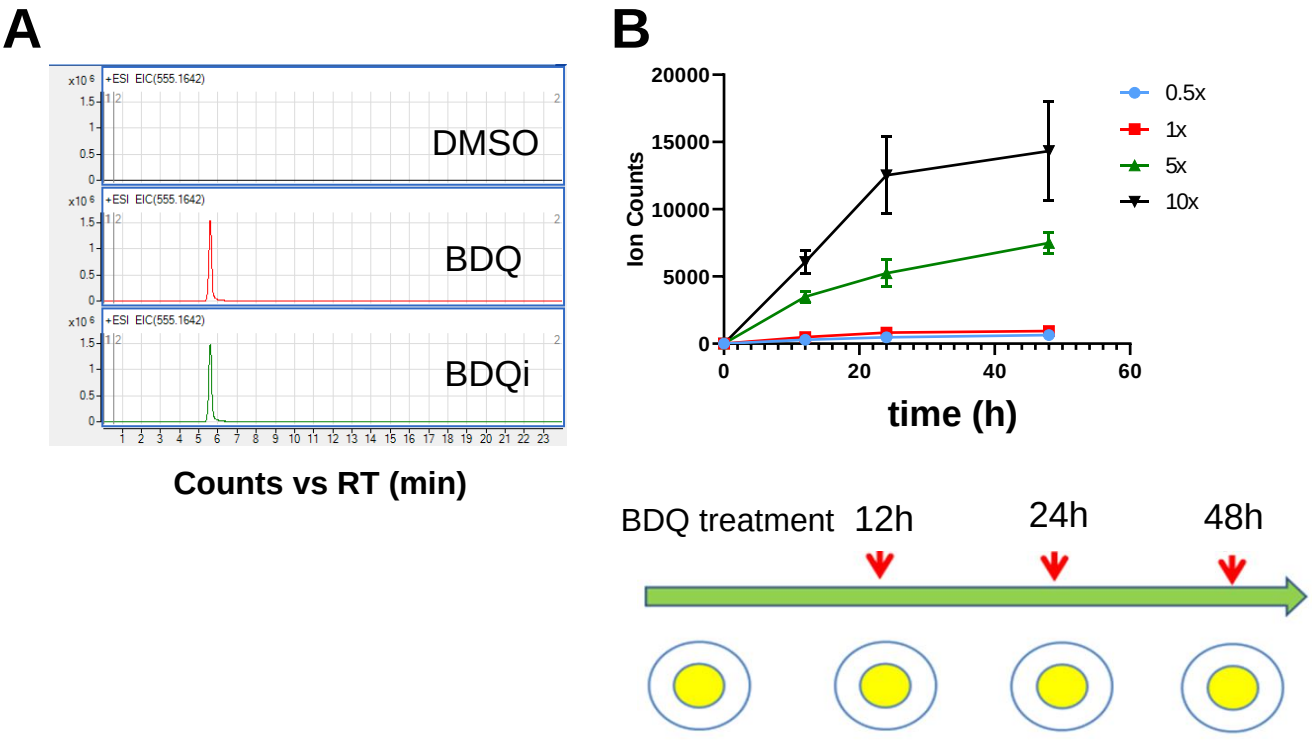

Fig. S1. The intrabacterial accumulation of BDQ during treatment. (*A*) EIC for intrabacterial accumulated BDQ (50X MIC, *m/z* = 555.1642 $[M+H]^+$) and BDQi (equimolar range as BDQ, *m/z* = 555.1642 $[M+H]^+$), after 24h treatment. (*B*) Line graph indicating the abundance of intrabacterial level of BDQ compound following expoure of wild-type Mtb H37Rv to the antibiotics, at a serie of dose (0-10X MIC) over time (0-48h).

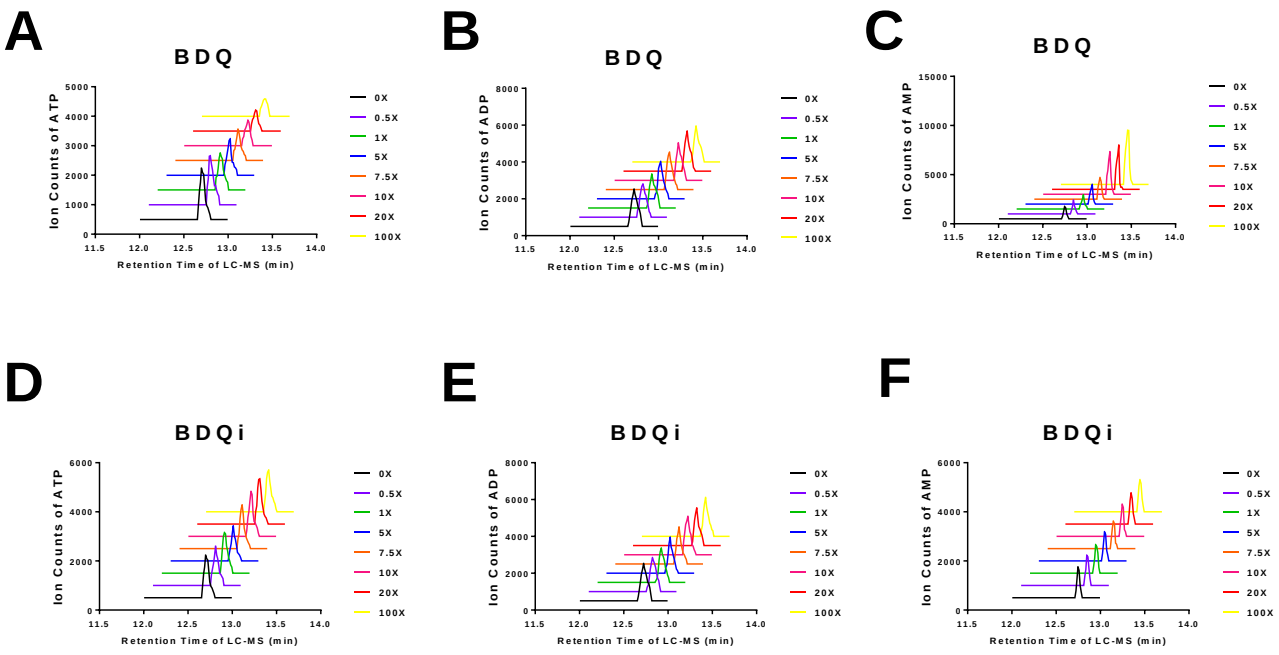

Fig. S2. Kinetic analysis of BDQ's impact on intrabacterial AXP. (*A*, *D*) EIC for ATP (*m/z* = 505.9885 $[M-H]^-$) during the BDQ or BDQi dose-dependent treatment. (*B*, *E*) EIC for ADP (*m/z* = 426.0221 $[M-H]^-$) during the BDQ or BDQi dose-dependent treatment. (*C*, *F*) EIC for AMP (*m/z* = 346.0558 $[M-H]^-$) during the BDQ or BDQi dose-dependent treatment. All data points represent the average of 3 technical replicates and are representative of 2 independent experiments.

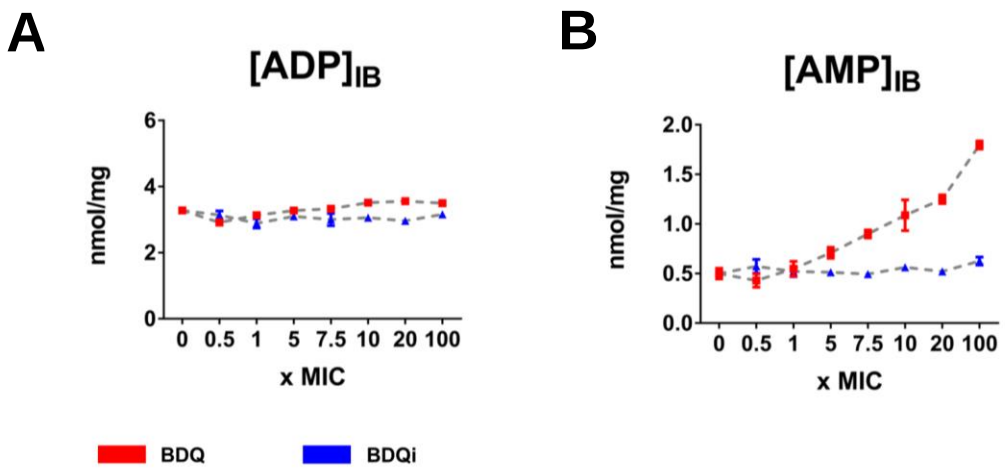

Fig. S3. Impact of BDQ on intrabacterial pools of ADP and AMP in Mtb H37Rv. Line graph indicating the abundance of intrabacterial ADP (*A*) or AMP (*B*) following exposure of wild-type Mtb H37Rv to BDQ or BDQi. All data points represent the average of 3 technical replicates and are representative of 2 independent experiments.

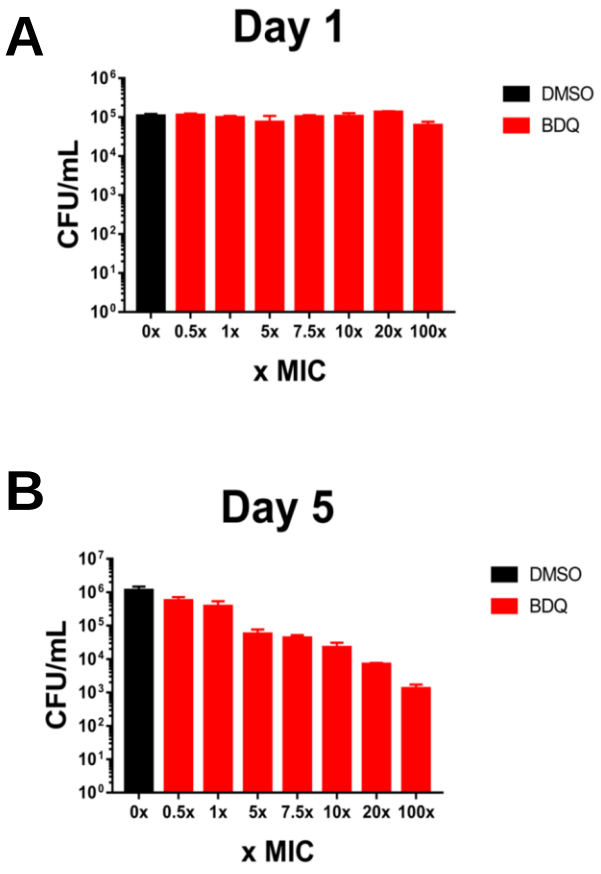

Fig. S4. Delayed bactericidal activity of BDQ. CFU-based readout of Mtb viability measurement following 1d (*A*) or 5d (*B*) exposure to BDQ. All data points represent the average of 3 technical replicates and are representative of 2 independent experiments.

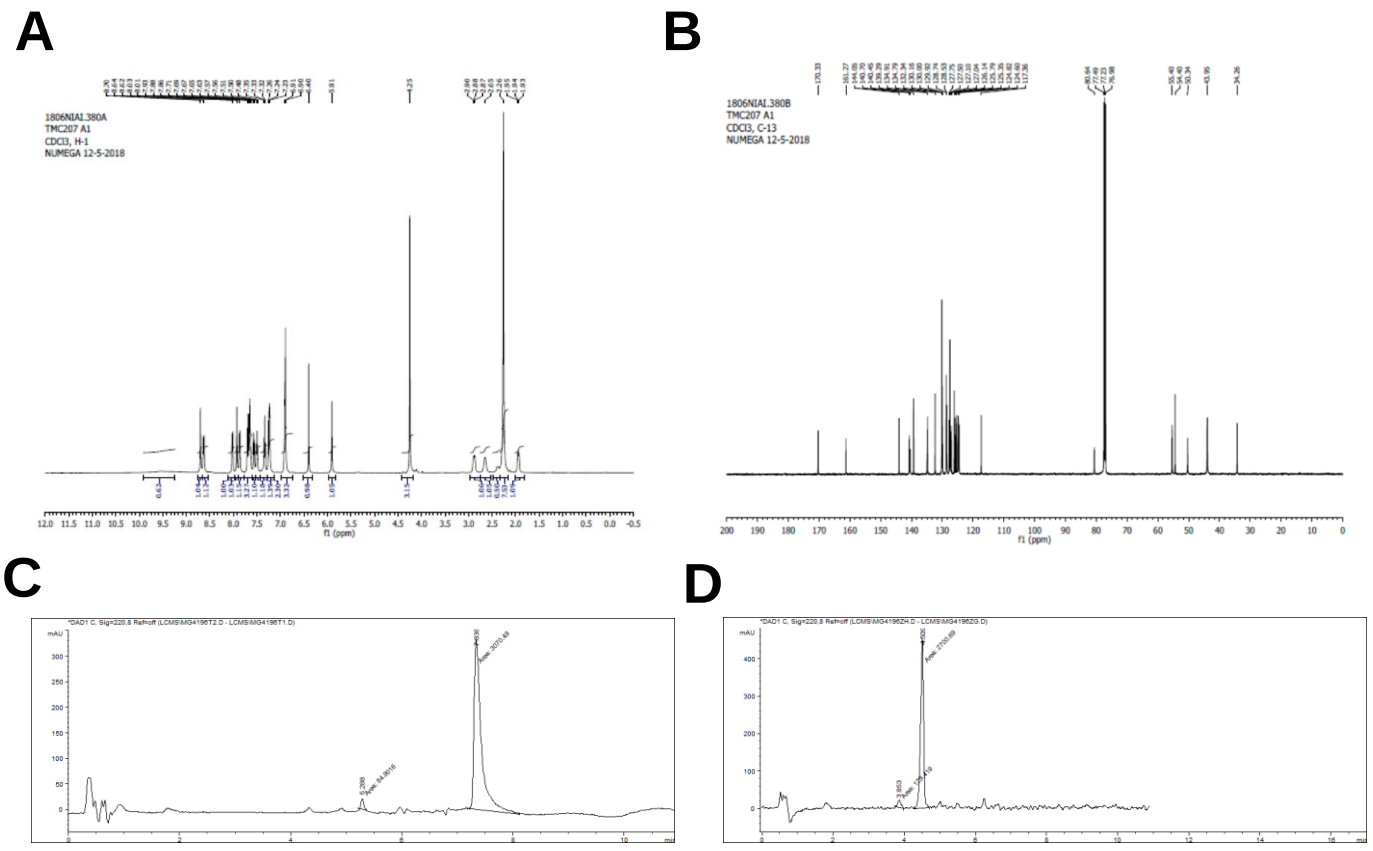

Fig. S5. Characterization data for synthesized Bedaquiline fumarate salt (BDQ). (*A*) The ^{1}H-NMR spectra of BDQ. ^{1}H NMR (500 MHz, $CDCl_3$) δ: 9.57 (br s, 1H), 8.70 (s, 1H), 8.63 (d, 1H, *J* = 8.0), 8.02 (d, 1H, *J* = 10.0), 7.93 (s, 1H), 7.87 (d, 1H, *J* = 10.0), 7.71-7.54 (m, 3H),7.57 (d, 1H, *J* = 5.0), 7.50 (t, 1H, *J* = 7.5), 7.33 (t, 1H, *J* =7.5), 7.24-7.23 (m, 2H), 6.91-6.90 (m, 3H), 6.40 (s, 1H), 5.91 (s, 1H), 4.25 (s, 3H), 2.90-2.87 (m, 1H), 2.65 (br s, 1H), 2.26 (br s, 8H), 1.94 (p, 1H, *J* = 5.0). (*B*) The ^{13}C-NMR spectra of BDQ. ^{13}C NMR (125 MHz, $CDCl_3$) δ: 170.3, 161.3, 144.1, 140.7, 140.5, 139.3, 134.9, 134.8, 132.3, 130.2, 130.0, 129.9, 128.7, 128.5, 127.8, 127.5, 127.0, 126.1, 125.8, 125.4, 124.8, 124.6, 117.4, 80.6, 55.4, 54.4, 50.3, 44.0, 34.3. (*C*) HPLC purity determination by Method A-97.3% (220 nm detection). In Method A, the chemical is analyzed by Phenomenex Kinetex PFP 2.6 µm 100 Å column. The mobile phase includes solvent A (10mM Ammonium formate in water) and solvent B (Methanol). The gradient is: 0 min, 50% B; 0-5 min, 95% B; 5-11 min, 95% B. (*D*) HPLC purity determination by Method B-95.4% (220 nm detection). In Method B, the chemical is analyzed by Phenomenex Fusion-RP 4 µm 80 Å column. The mobile phase includes solvent A (1% Formic acid in water) and solvent B (1% Formic acid in acetonitrile). The gradient is: 0 min, 30% B; 0-5 min, 95% B; 5-11 min, 95% B.

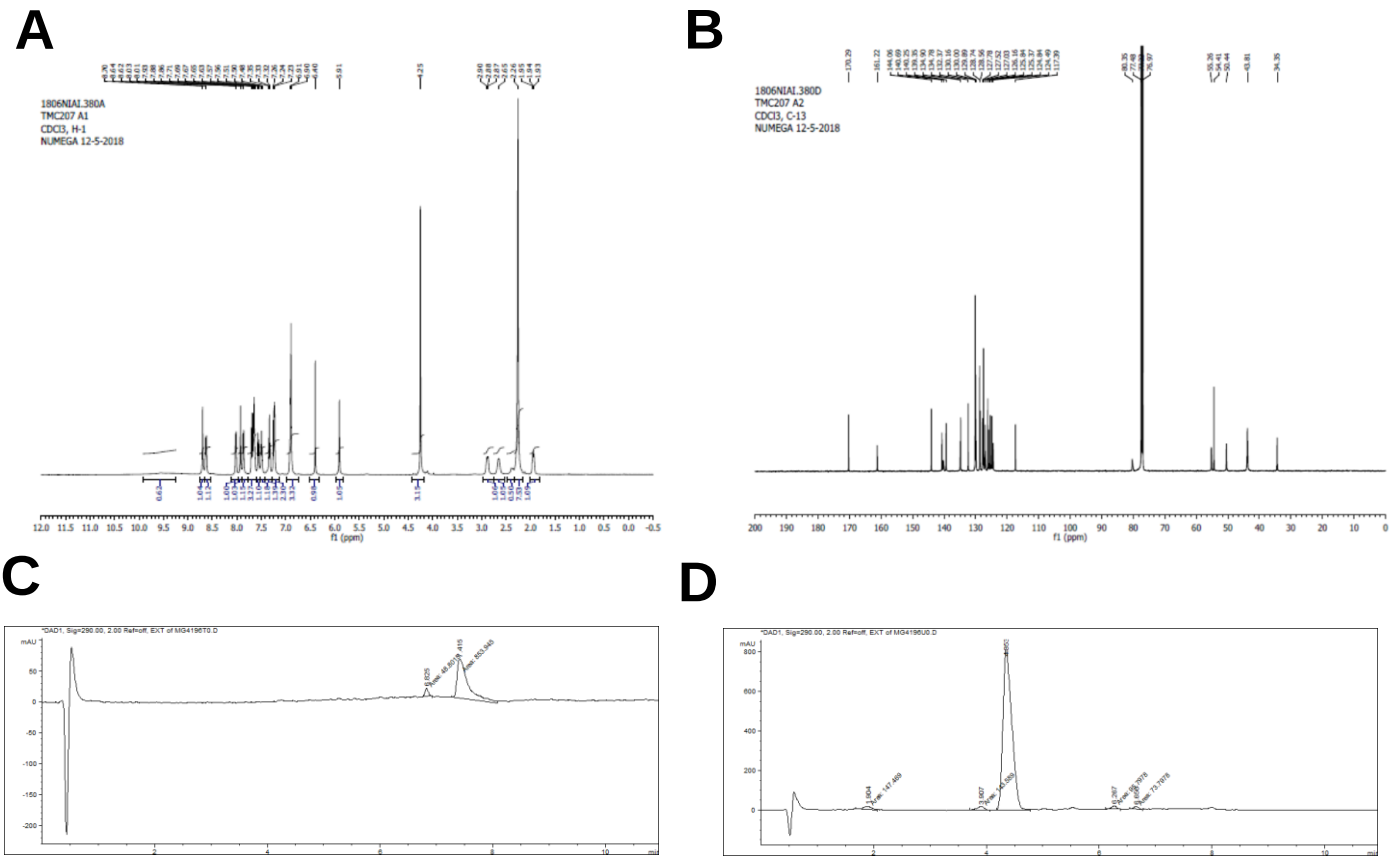

Fig. S6. Characterization data for synthesized Bedaquiline inactive enantiomer (BDQi). (*A*) The ^{1}H-NMR spectra of BDQi. ^{1}H NMR (500 MHz, $CDCl_3$) δ: 9.60 (br s, 1H), 8.63 (m, 1H, *J*= 10.0), 8.05 (d, 1H, *J* = 20.0), 7.91-7.85 (m, 2H), 7.69-7.54 (m, 3H), 7.54-7.48 (m, 2H), 7.34 (t, 1H, *J* =7.5), 7.27-7.25 (m, 2H), 6.93-6.89 (m, 3H), 6.40 (s, 1H), 5.90 (s, 1H), 4.25 (s, 3H), 2.90-2.87 (m, 1H), 2.65 (br s, 1H), 2.26 (br s, 8H), 1.94 (p, 1H, *J* = 5.0). (*B*) The ^{13}C-NMR spectra of BDQi. ^{13}C NMR (125 MHz, $CDCl_3$) δ: 170.3, 161.2, 144.1, 140.7, 140.3, 139.4, 134.9, 134.8, 132.4, 130.2, 130.0, 129.9, 128.7, 128.6, 127.8, 127.5, 127.0, 126.2, 135.8, 125.4, 124.8, 124.5, 117.3, 80.4, 55.3, 54.4, 50.4, 43.8, 34.4. (*C*) HPLC purity determination by Method A-94.5% (290 nm detection). In Method A, the chemical is analyzed by Phenomenex Kinetex PFP 2.6 µm 100 Å column. The mobile phase includes solvent A (10mM Ammonium formate in water) and solvent B (Methanol). The gradient is: 0 min, 50% B; 0-5 min, 95% B; 5-11 min, 95% B. (*D*) HPLC purity determination by Method B-95.1% (290 nm detection). In Method B, the chemical is analyzed by Phenomenex Fusion-RP 4 µm 80 Å column. The mobile phase includes solvent A (1% Formic acid in water) and solvent B (1% Formic acid in acetonitrile). The gradient is: 0 min, 30% B; 0-5 min, 95% B; 5-11 min, 95% B.

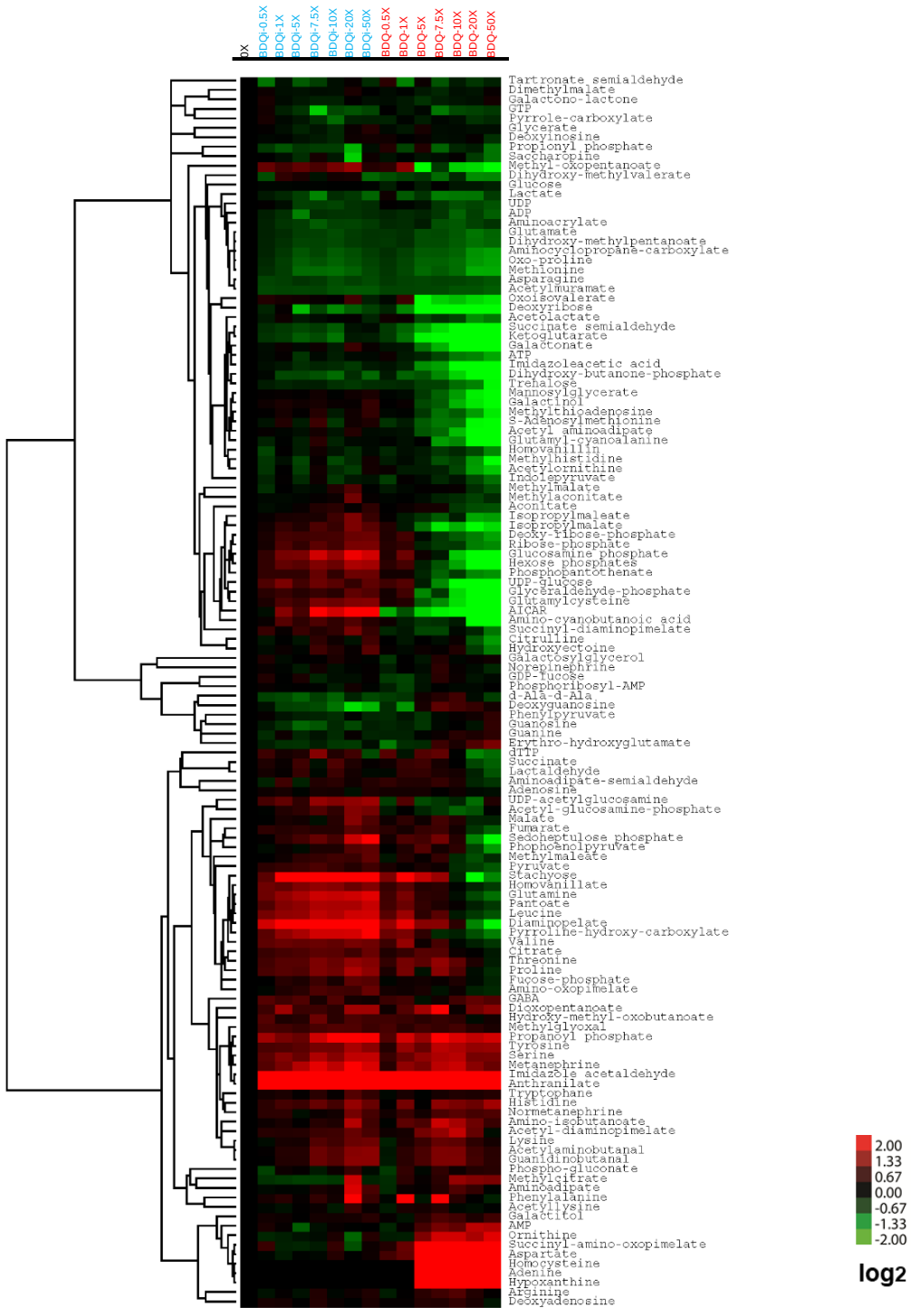

Fig. S7. Heatmap profile following 1d exposure of Mtb to BDQ or BDQi. Metabolic profile that following 24h exposure of Mtb to BDQ or BDQi concentrations as indicated. Columns represent individual treatments as indicated. Rows denote individual metabolites measured. Data were parsed by uncentered Pearson's correlation with centroid linkage clustering and rendered using the image generation program Java TreeView (http://jtreeview.sourceforge.net/).

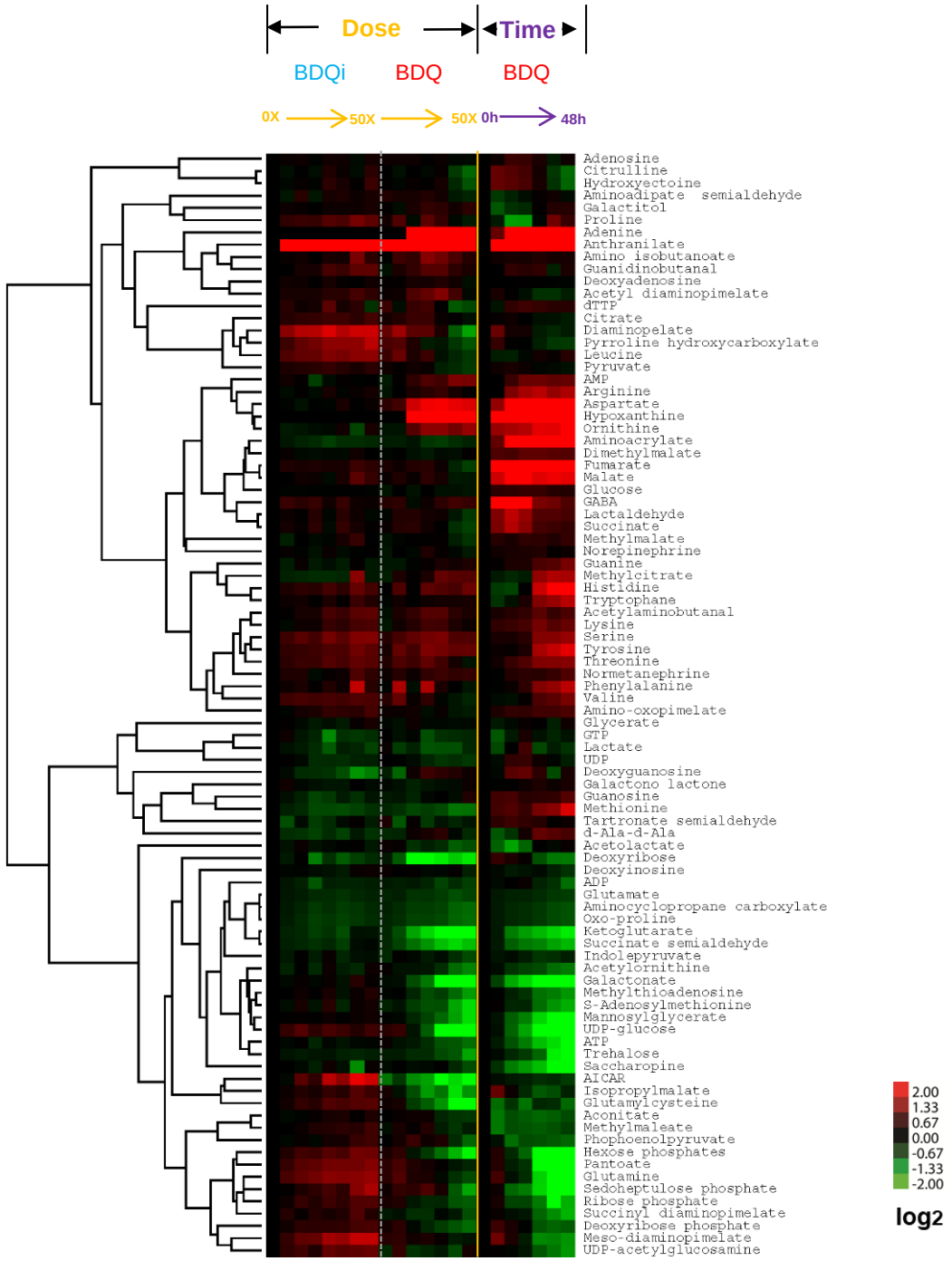

Fig. S8. Similarity of dose- and time- dependent metabolic changes triggered by BDQ. Co-cluster analysis of BDQ triggered metabolic changes following dose- and time-dependent exposures. Dose-dependent analysis was conducted following 24h exposure of Mtb to BDQ or BDQi concentration as indicated. Time-dependent analysis was conducted over time (0-48h) using BDQ at 50X MIC. Data were parsed by uncentered Pearson's correlation with centroid linkage clustering and rendered using the image generation program Java TreeView (http://jtreeview.sourceforge.net/).

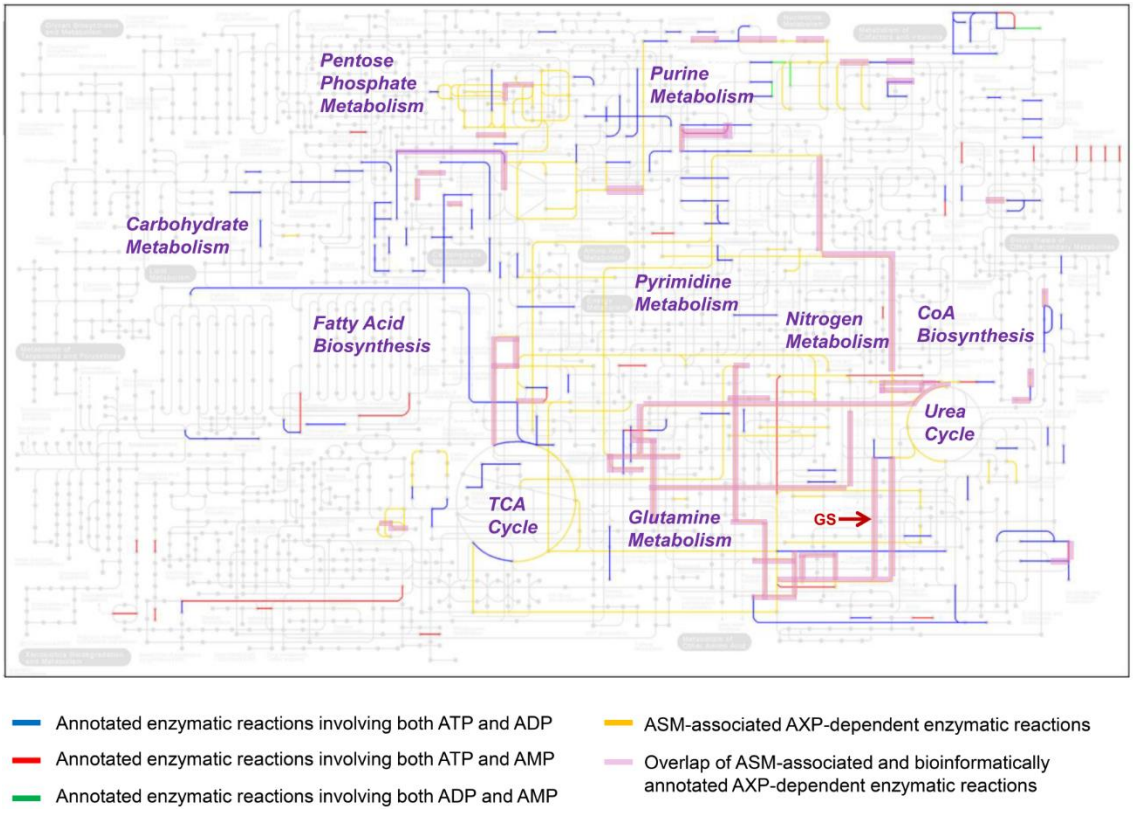

Fig. S9. Overlap of BDQ associated activity-specific metabolites with bioinformatically annotated AXP-dependent reactions. Blue lines depict annotated enzymatic reactions that involve ATP and ADP as substrate and product. Red lines depict annotated enzymatic reactions that involve ATP and AMP as substrate and product. Green lines depict annotated enzymatic reactions that involve ADP and AMP as substrate and product. A detailed list of annotated AXP-dependent enzymatic reactions is presented in Table S1. Gold lines indicate annotated enzymatic reactions in which BDQ ASMs (G1, G2, G3, G4) serve as substrate or product, or are inhibited by these metabolites. A detailed list of these enzymatic reactions is presented in Table S3. Pink transparent lines denote enzymatic reactions identified by bioinformatics annotation (blue, red and green lines) and experimental ASMs (gold lines). Italicized text highlights statistically enriched metabolic modules. “GS” identifies the glutamine synthetase catalyzed-reaction in Mtb metabolome.

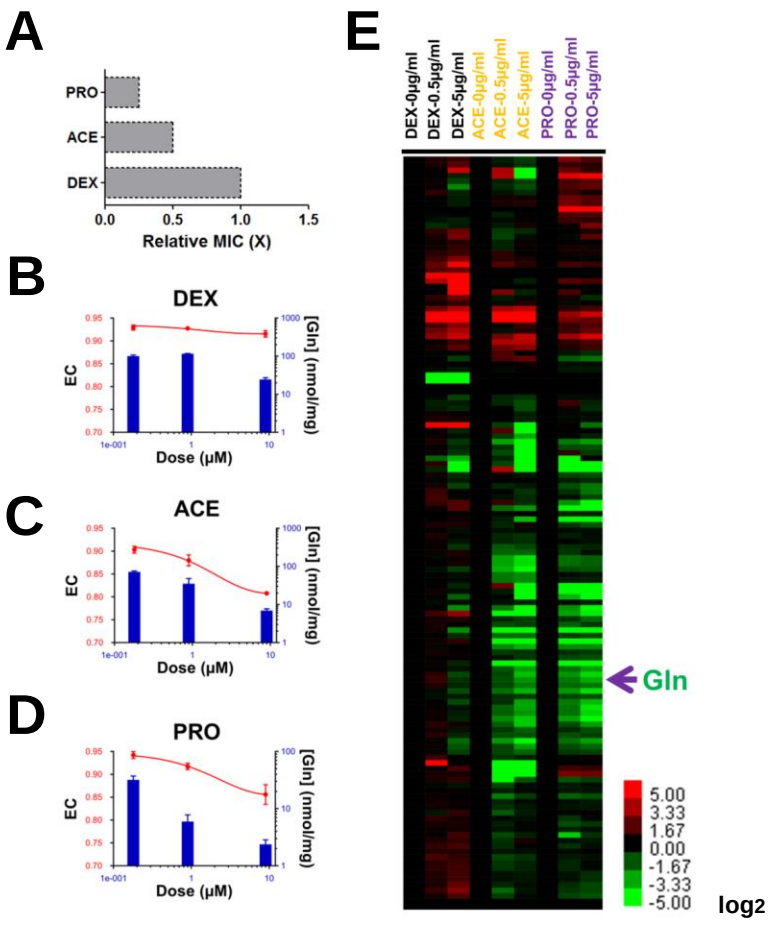

Fig. S10. Carbon source-dependence of BDQ activity and correlation with EC and glutamine abundance. (*A*) BDQ activity in different carbon sources as reported by the recovery of enumerable MIC on 7H10 agar plates. PRO indicates 0.2% propionate; ACE indicates 0.2% acetate; DEX indicates 0.2% dextrose as the sole carbon source provided; (*B, C, D*) Overlay plots of BDQ induced changes in EC and intracellular glutamine abundance following exposure of Mtb to different carbon sources as indicated. Left y-axis is EC, the right y-axis is glutamine level (nmol/mg), and the x-axis is the dose of BDQ (μM); (*E*) Carbon source-specific effects of BDQ on the Mtb metabolome. Data are depicted on a $\log_2$ scale relative to untreated control for BDQ. All data points represent the average of 3 technical replicates and are representative of 2 independent experiments.

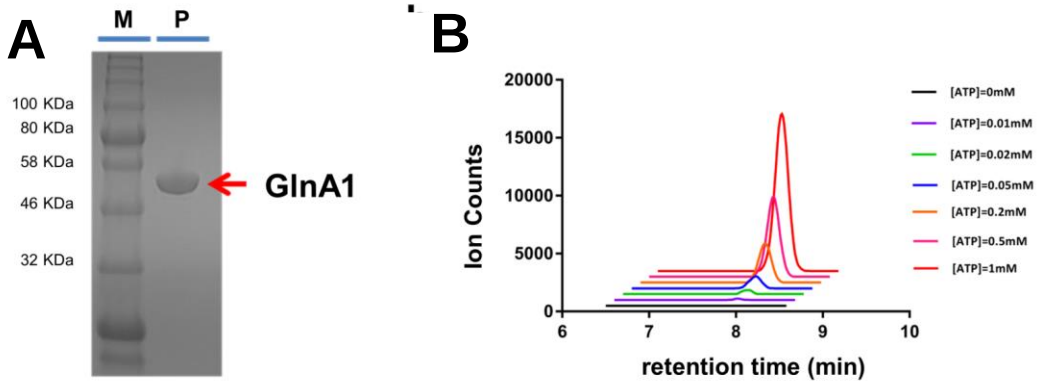

Fig. S11. *In vitro* overexpression, purification and activity of recombinant Mtb GlnA1. (*A*) Overexpression and purification of recombinant Mtb GlnA1 from *E.coli*. M denotes protein markers (11–245 kDa, P7712S, NEB), P denotes target protein; (*B*) *in vitro* activity of Mtb GlnA1 activity as monitored by LC-MS. The different colors of lines show EIC of Glutamine (*m/z* = 145.0619 [M-H]-) using different ATP concentrations in the reaction systems. All data points represent the average of 3 technical replicates and are representative of 2 independent experiments.

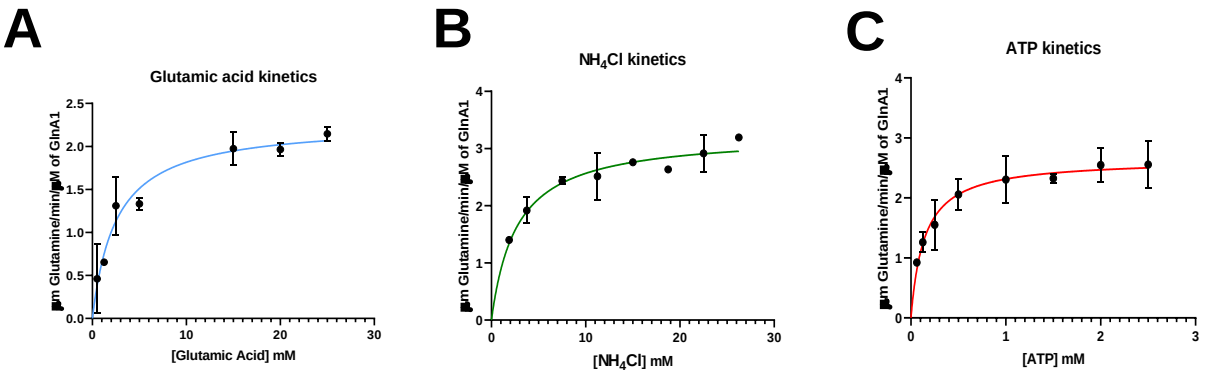

D

Substrates	K_m (mM)	V_{max} (μM glutamine/min/μM of GlnA1)
Glutamic acid	2.538 ± 0.5624	2.277 ± 0.1307
NH_4Cl	2.688 ± 0.5457	3.255 ± 0.1344
ATP	0.1423 ± 0.02844	2.643 ± 0.1130

Fig. S12. Kinetic parameters (Km and Vmax) measurement for the glutamine synthetase activity of Mtb GlnA1. (*A*) The fitted curve of GlnA1 enzymatic activity when varying the concentration of glutamic acid in reaction system. (*B*) The fitted curve of GlnA1 enzymatic activity when varying the concentration of NH_4Cl in reaction system. (*C*) The fitted curve of GlnA1 enzymatic activity when varying the concentration of ATP in reaction system. (*D*) The calculated Km and Vmax values of Mtb GlnA1 for substrate glutamic acid, NH_4Cl and ATP.

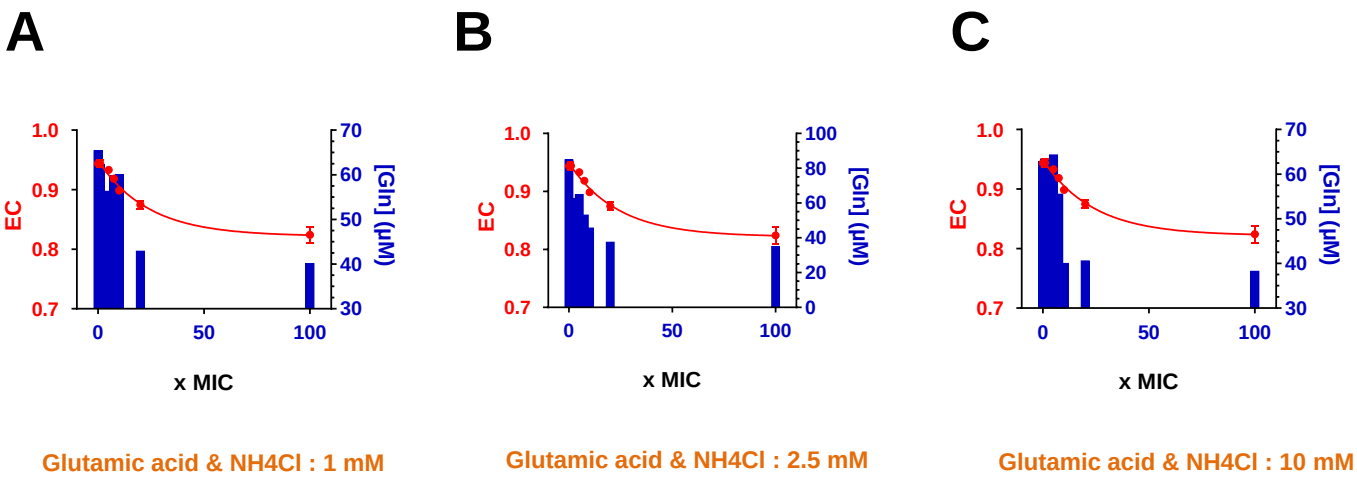

Fig. S13. EC dependence of Mtb GlnA1 enzymatic activity at different substrate concentrations. Overlay plot of BDQ treatment on the EC of viable Mtb (left y-axis) and *in vitro* activity of Mtb GlnA1 (right y-axis) in the presence of the *in vitro* AXP ratio corresponding to the same range of BDQ concentrations. (*A*) Using substrate concentrations (1 mM for both glutamic acid and NH_4Cl) below their Km values. (*B*) Using Km substrate concentrations (2.5 mM for both glutamic acid and NH_4Cl). (*C*) Using substrate concentrations (10mM for both glutamic acid and NH_4Cl) higher than their Km values.

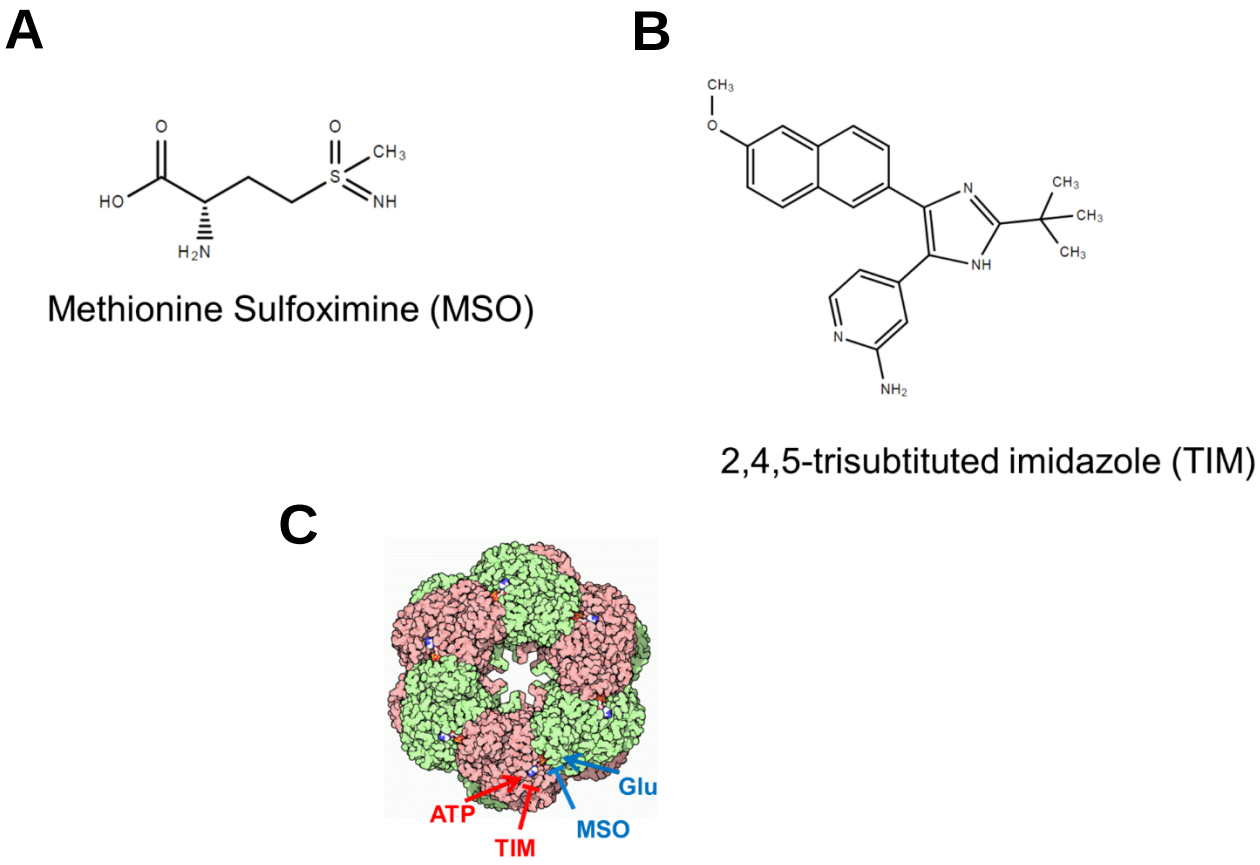

Fig. S14. Molecular structure of GS and predicted binding sites of MSO and TIM. (*A*) Molecular structure of Methionine Sulfoximine (MSO). (*B*) Molecular structure of 2,4,5-trisubstituted imidazole (TIM). (*C*) A schematic 3D structure of Mtb GlnA1 with red arrow pointing to the ATP binding site; and blue arrow pointing to the glutamate binding site. TIM is a GS inhibitor that competes for the ATP binding site, MSO is a GS inhibitor competes for the glutamate binding site.

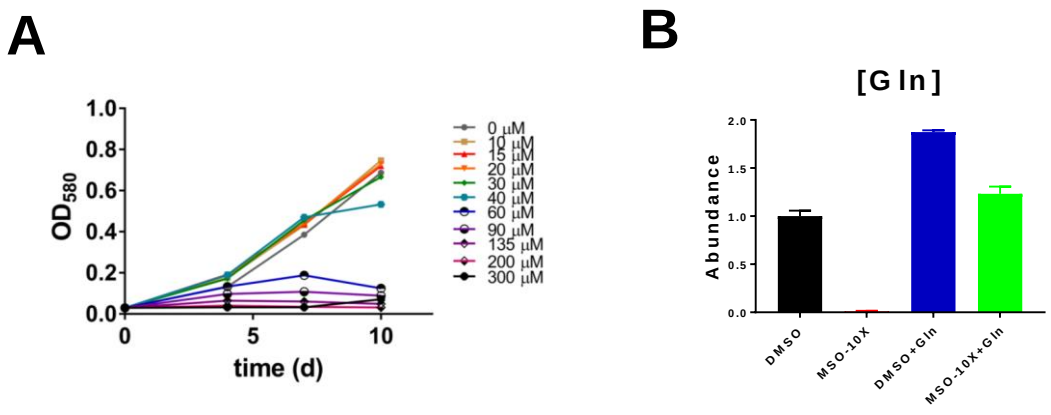

Fig. S15. MSO-mediated inhibition of Mtb growth and intracellular glutamine synthesis. (*A*) Growth curves of Mtb in the presence of a dose range of MSO (0-300 µM), as reported by OD_{580} value. (*B*) Bar graph indicating intracellular glutamine abundance following exposure of wild type Mtb H37Rv to MSO (10X MIC), in 7H10 medium or 7H10 medium supplemented with 5 mM glutamine. All data points represent the average of 3 technical replicates and are representative of 2 independent experiments.

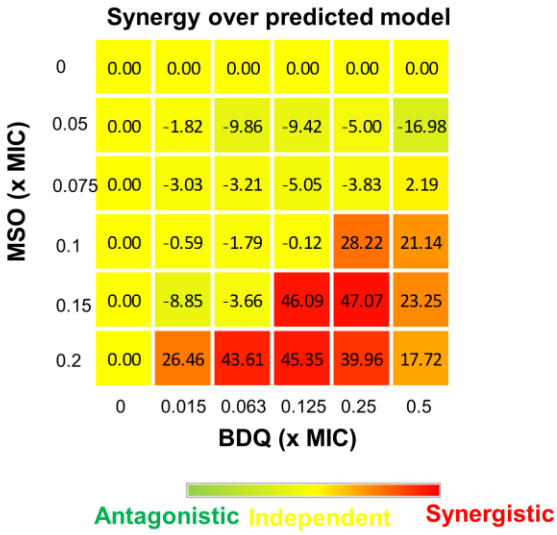

Fig. S16. Synergy-antagonism matrix of the BDQ-MSO drug pair. Each measurement was compared to expected values derived from the single-agent data along the left and bottom edges of the matrix. In each well, positive values represent the strength of synergistic effects while negative values represent antagonistic effects. The color green is used to depict antagonism, while yellow depicts indifference, and red depicts synergy.

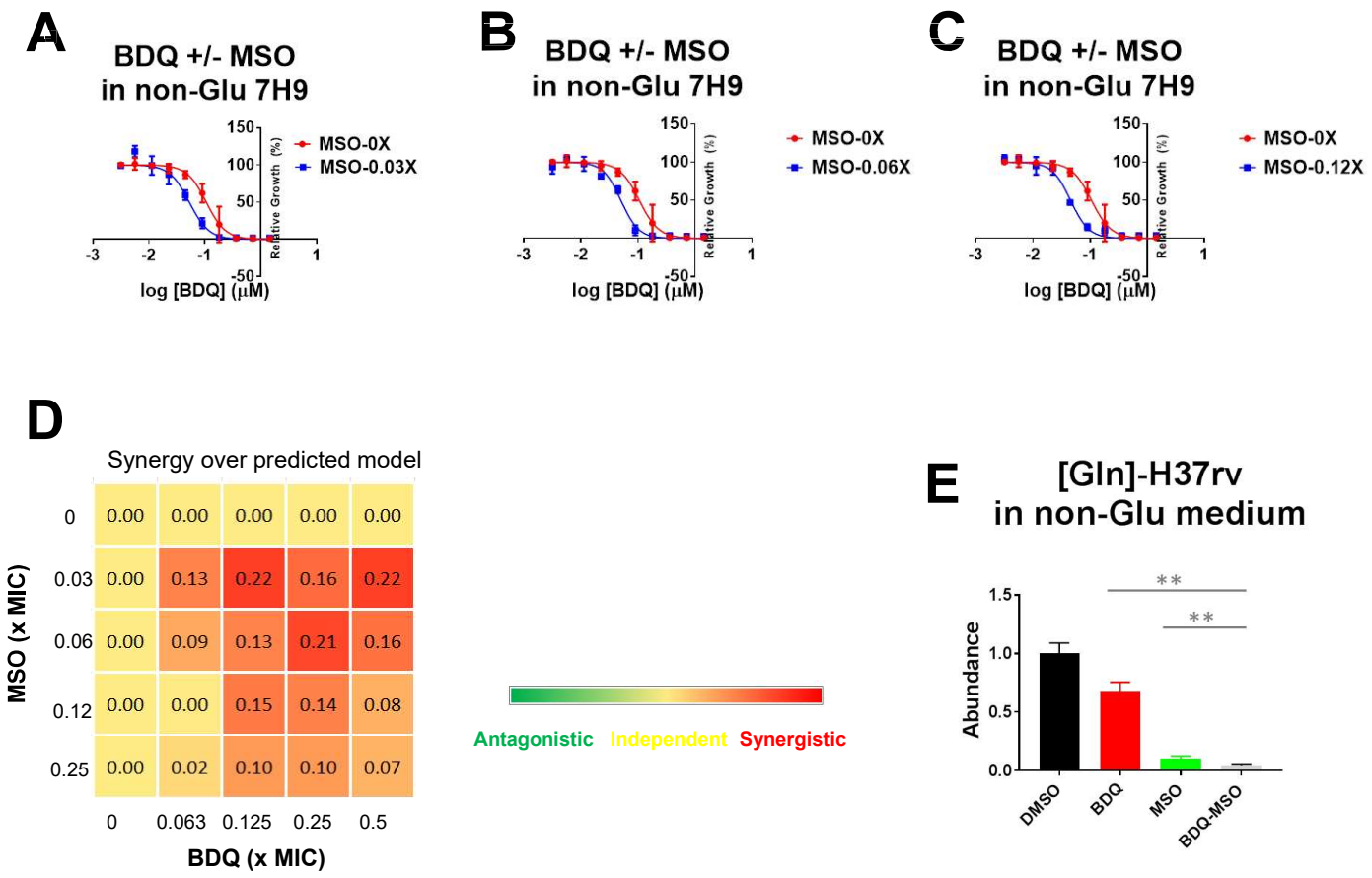

Fig. S17. Synergistic inhibition of Mtb growth and glutamine pools by BDQ and MSO in non-Glu medium. (*A, B, C*) Mtb strain H37rv growth inhibition curves of BDQ in the absence (red) and presence (blue) of varying concentrations of MSO (*A*, 0.03X MIC; *B*, 0.06X MIC; *C*, 0.12X MIC). Curves depict OD_{580} values following 10d incubation in non-Glu 7H9 liquid medium with 0.2% glucose and 0.2% glycerol as carbon sources and drugs as indicated, the raw values of IC50 and ΔIC50 are listed in Table S6. (*D*) Synergy-antagonism matrix of the BDQ-MSO drug pair in non-Glu 7H9 broth. Each measurement was compared to expected values derived from the single-agent data along the left and bottom edges of the matrix. In each well, positive values represent the strength of synergistic effects while negative values represent antagonistic effects. The color green is used to depict antagonism, while yellow depicts indifference, and red depicts synergy. (*E*) Total bacterial glutamine pools following exposure of Mtb to BDQ (20X MIC), MSO (1X MIC) or the combination. ** $p < 0.01$ by unpaired Student t-test. All data points represent the average of at least 2 replicates.

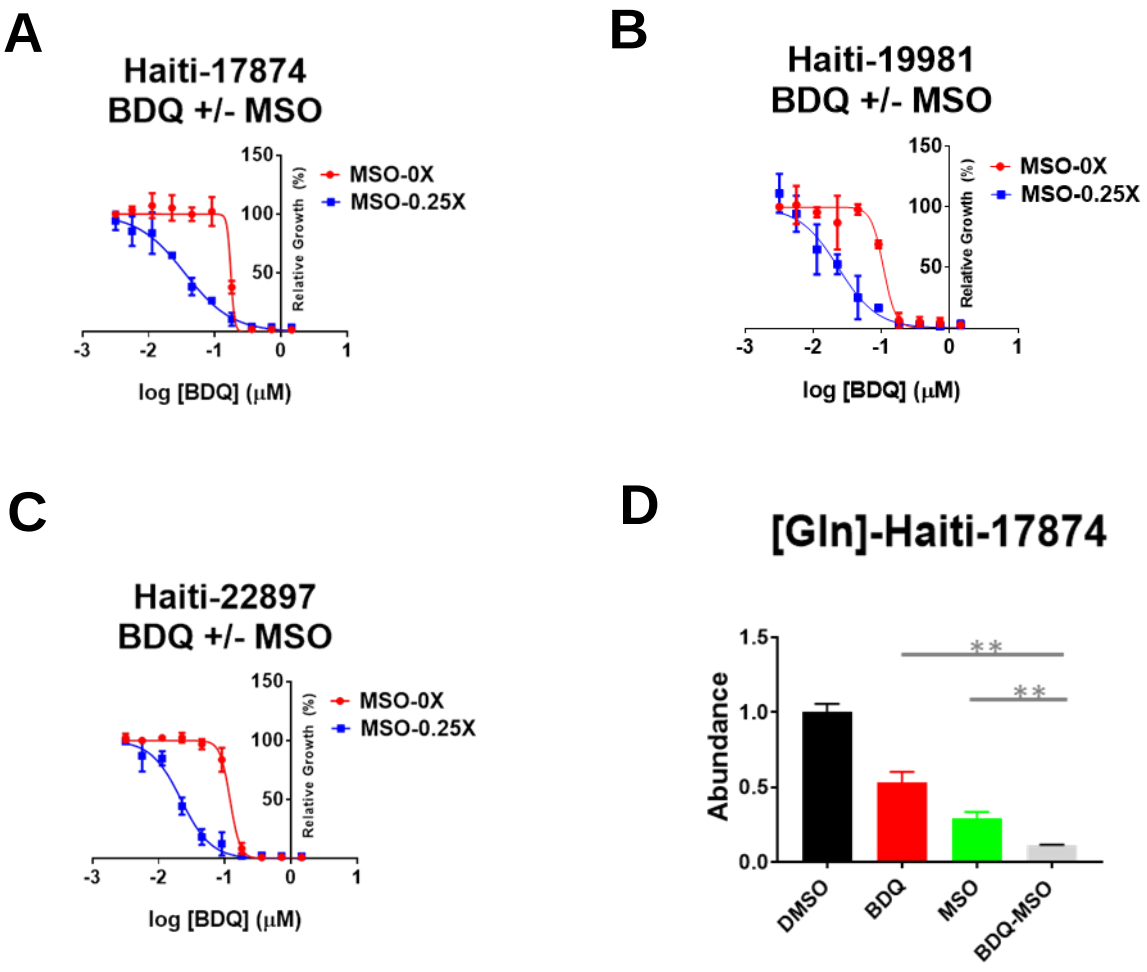

Fig. S18. Synergistic inhibition of bacterial growth and glutamine pools by BDQ and MSO in clinical Mtb isolates from Haiti. (*A, B, C*) Clinical Mtb strains (Haiti-17874, -19981, -22897) growth inhibition curves of BDQ in the absence (red) and presence (blue) of of MSO (0.25X MIC). Curves depict OD580 values following 10d incubation in regular 7H9 liquid medium with 0.2% glucose and 0.2% glycerol as carbon sources and drugs as indicated, the raw values of IC50 and ΔIC50 are listed in Table S6. (*D*) Total bacterial glutamine pools following exposure of Mtb to BDQ (20X MIC), MSO (1X MIC) or the combination in Haiti-17874 background. ** $p < 0.01$ by unpaired Student t-test.

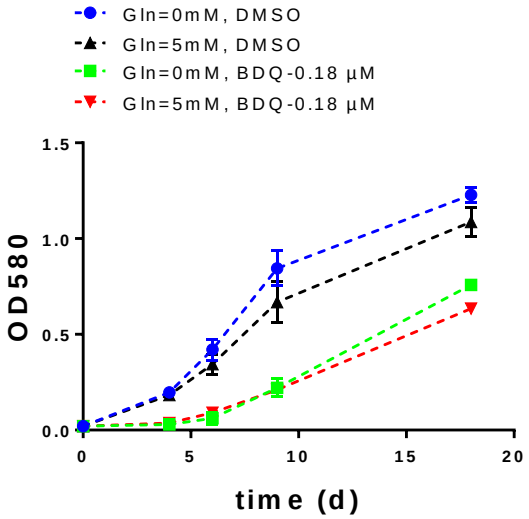

Fig. S19. Inability of glutamine to antagonize BDQ activity. Mtb growth curves in the absence and presence of BDQ (0.18 µM) in 7H9 liquid media either lacking or supplemented with exogenous glutamine (5 mM).

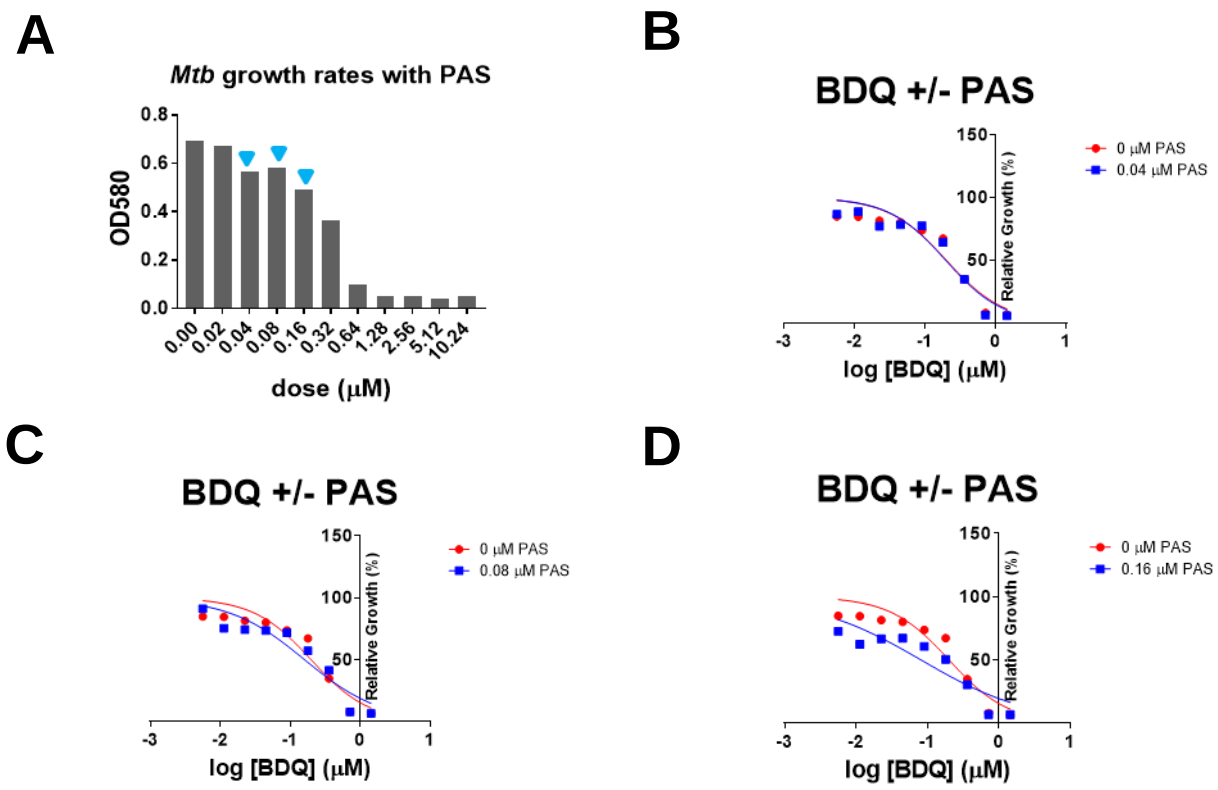

Fig. S20. BDQ indifference to PAS, an inhibitor of folate metabolism. (*A*) Growth inhibitory effects of *para*-aminosalicylic acid (PAS) on Mtb. Inverted triangles indicate sub-inhibitory concentrations selected for use in BDQ-PAS combination experiments. (*B, C, D*) Growth inhibitory effects of PAS (0.04 μM in *B*, 0.08 μM in *C*, 0.16 μM in *D*) in combination with BDQ.

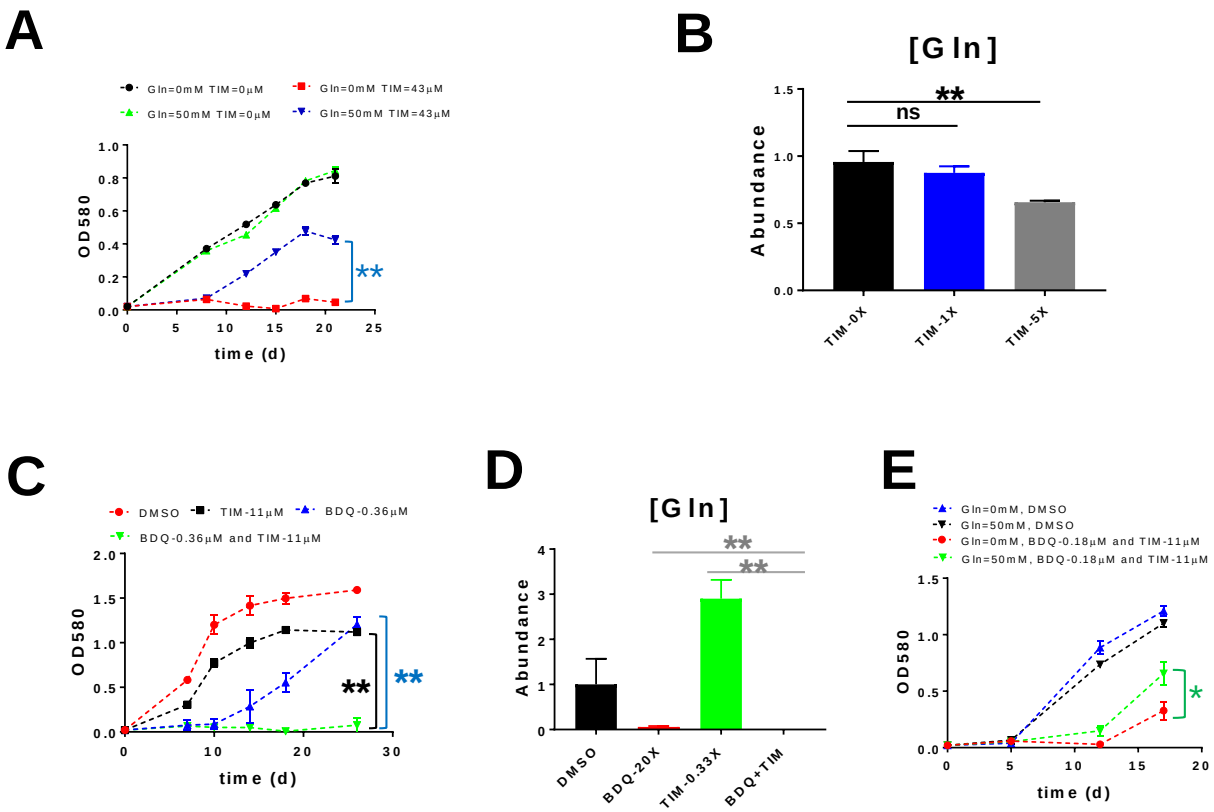

Fig. S21. TIM-mediated inhibition of Mtb growth, GS activity and glutamine synthesis. (*A*) Mtb growth inhibition by TIM (43 µM) and reversibility with exogenous glutamine (50 mM), in 7H9 liquid media containing acetate (0.2%, w/v) as sole supplied carbon source; (*B*) TIM's impact on bacterial glutamine pool. (*C*) Mtb growth curves in the absence and presence of TIM (11 µM), BDQ (0.36 µM) or a combination of TIM and BDQ in 7H9 liquid medium with 0.2% glucose and 0.2% glycerol as carbon sources. (*D*) Intrabacterial glutamine levels following 3d exposure of Mtb for BDQ, TIM or the combination as indicated. (*E*) Partial rescue of BDQ (0.18 µM)-TIM (11 µM) combination with exogenous (50 mM) glutamine. ns = not significant; ** $p < 0.01$; * $0.01 < p < 0.05$ by unpaired Student t-test. All data points represent the average of 3 technical replicates and are representative of 2 independent experiments.

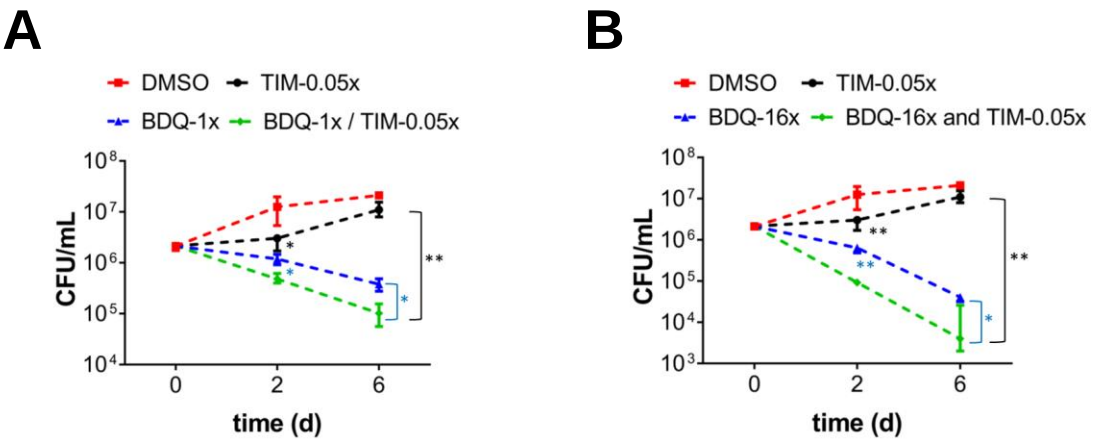

Fig. S22. BDQ-TIM-mediated killing of Mtb. (*A*) CFU-based assay of Mtb viability following exposure to TIM (0.05X MIC), BDQ (1X MIC) or the combination; (*B*) same as panel (*A*) except TIM (0.05X MIC) and BDQ (16X MIC); All data points represent the average of 3 technical replicates and are representative of 2 independent experiments. ** $p < 0.01$; * $0.01 < p < 0.05$ by unpaired Student t-test.

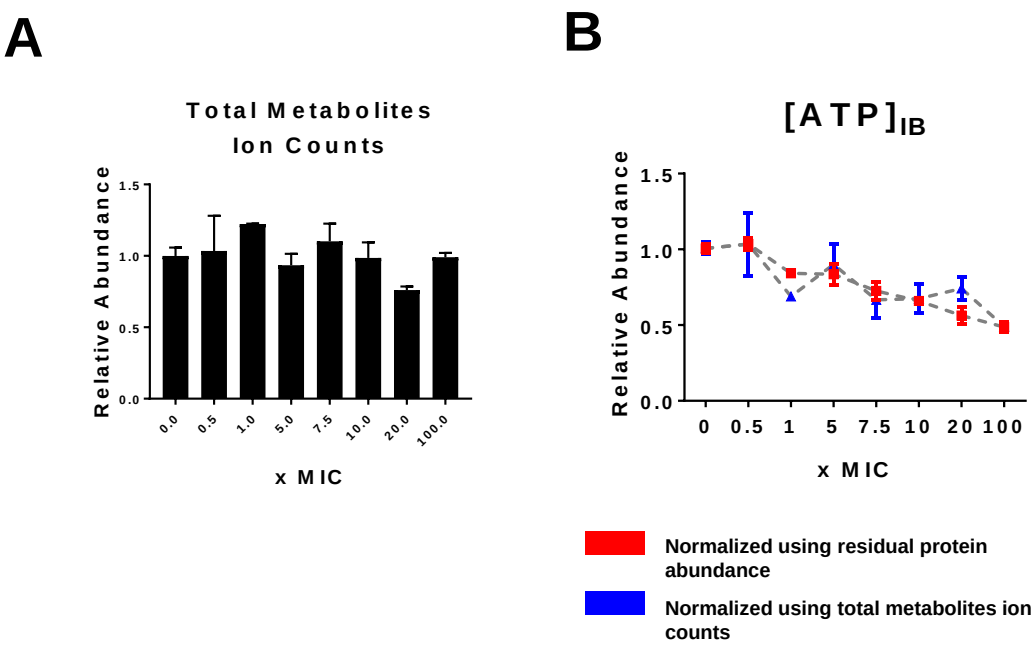

Fig. S23. The comparison of different metabolomics samples normalization methods. (*A*) The relative abundance of total metabolites ion counts (based on total 130 metabolites) in the dose- dependent BDQ treatment samples. (*B*) The comparison of computed ATP abundance by using residual protein abundance and using total metabolites ion counts.

Additional data table S1-6 (separate file)

Table. S1. Annotated AXP-associated enzymatic reactions in the Mtb genome. This table lists ATP-ADP, ATP-AMP or ADP-AMP dependent reactions in the annotated genome of Mtb H37Rv. Table columns include KEGG orthology (k numbers), enzyme commission (EC numbers) and annotated gene functions.

Table. S2. Pathway enrichment analysis based on AXP-associated enzymatic reactions. Pathway enrichment analysis using Mtb genome-encoded AXP-associated enzymatic reactions as an input for Gene Ontology Consortium (http://www.geneontology.org/). "Hits in Mtb genome" indicate the gene numbers of specific GO in Mtb whole genome. "Hits in input list" indicate the gene numbers in our input AXP-associated gene list. "Fold enrichment" means the strength of enrichment over the averaged theoretical value of specific GO. We used $p < 0.05$ as a cut-off to select the statistic significant GO items.

Table. S3. Annotated enzymatic reactions associated with BDQ ASM. Columns with orange fillings indicate enzymatic reactions that use above ASMs as substrates or products. Columns with green fillings are enzymatic reactions with published evidence of biochemical inhibition by ATP, ADP or AMP.

Table. S4. Pathway enrichment analysis of BDQ activity-specific metabolic effects. Pathway enrichment analysis using BDQ activity-specific metabolites with MetaboAnalyst 3.0 (http://www.metaboanalyst.ca/). "Hits" indicate metabolites exhibiting pathway enrichment, "p" means p-value, "-log(p)" means the reciprocal $\log_2$ transformed version of p-value, "FDR" is the computed false discovery rate. The colored text represents statistically enriched metabolic pathways with FDR < 0.05.

Table. S5. Pairwise PCC values of Mtb activity-specific metabolites under difference energy statues. Computed pairwise Pearson correlation coefficient matrix among BDQ activity-specific metabolites.

Table. S6. The computed IC_{50} and ΔIC_{50} values from the combination of BDQ and MSO, TIM and Btz043. The IC_{50} and ΔIC_{50} values were computed using GraphPad Prism 7.0. All data points represent the average of at least 3 replicates. P-values were calculated by unpaired Student t-test.